



ELSEVIER

Astroparticle Physics 17 (2002) 151–165

Astroparticle
Physics

www.elsevier.com/locate/astropart

Results from the ARGO-YBJ test experiment ARGO-YBJ Collaboration

C. Bacci^a, K.Z. Bao^b, F. Barone^c, B. Bartoli^c, P. Bernardini^d, S. Bussino^a,
E. Calloni^c, B.Y. Cao^e, R. Cardarelli^f, S. Catalanotti^c, S. Cavaliere^c, F. Cesaroni^d,
P. Creti^d, Danzengluobu^g, B. D’Ettorre Piazzoli^c, M. De Vincenzi^a,
T. Di Girolamo^c, G. Di Sciascio^{c,*}, Z.Y. Feng^h, Y. Fu^e, X.Y. Gaoⁱ, Q.X. Gengⁱ,
H.W. Guo^g, H.H. He^j, M. He^c, Q. Huang^h, M. Iacovacci^c, N. Iucci^a, H.Y. Jai^h,
C.L. Jing^j, F.M. Kong^e, H.H. Kuang^j, Labaciren^g, B. Li^b, J.Y. Li^e, Z.Q. Liuⁱ,
H. Lu^j, X.H. Ma^j, G. Mancarella^d, S.M. Mari^a, G. Marsella^d, D. Martello^d,
X.R. Meng^g, L. Milano^c, J. Muⁱ, M. Panareo^d, Z.R. Peng^j, P. Pistilli^a,
R. Santonico^f, P.R. Shen^j, C. Stanescu^a, L.R. Sun^b, S.C. Sun^b, A. Surdo^d,
Y.H. Tan^j, S. Vernetto^k, C.R. Wang^e, H. Wang^j, H.Y. Wang^j, Y.N. Wei^b,
H.T. Yang^j, Q.K. Yao^b, G.C. Yu^h, X.D. Yue^b, A.F. Yuan^g, M. Zha^j,
H.M. Zhang^j, J.L. Zhang^j, N.J. Zhang^e, X.Y. Zhang^e, Zhaxisangzhu^g,
Zhaxiciren^g, Q.Q. Zhu^j

^a INFN and Dipartimento di Fisica dell’Università di Roma Tre, 00146 Rome, Italy

^b Zhengzhou University, 450052 Henan, China

^c INFN and Dipartimento di Fisica dell’Università di Napoli, 80125 Napoli, Italy

^d INFN and Dipartimento di Fisica dell’Università di Lecce, 73100 Lecce, Italy

^e Shandong University, 250100 Jinan, China

^f INFN and Dipartimento di Fisica dell’Università di Roma “Tor Vergata”, 00133 Rome, Italy

^g Tibet University, 850000 Lhasa, China

^h South West Jiaotong University, 610031 Chengdu, China

ⁱ Yunnan University, 650091 Kunming, China

^j Cosmic Rays and High Energy Astrophysics Laboratory, IHEP, 100039 Beijing, China

^k Istituto di Cosmogeofisica del CNR and INFN, 10133 Torino, Italy

Received 6 July 2000; received in revised form 30 March 2001; accepted 30 May 2001

* Corresponding author. Fax: +39-81-676-246.

E-mail address: disciascio@na.infn.it (G.D. Sciascio).

Abstract

A resistive plate counters (RPCs) carpet of $\sim 50 \text{ m}^2$ has been put in operation in the Yangbajing Laboratory (Tibet, P.R. China) at 4300 m a.s.l., in order to study the RPCs performance at high altitude and the detector capability of imaging the EAS disc. This test has been performed in view of an enlarged use of RPCs for the ARGO-YBJ experiment. This experiment will be devoted to a wide range of fundamental issues in cosmic rays and astroparticle physics, including in particular γ -ray astronomy and γ -ray bursts physics at energies $\geq 100 \text{ GeV}$.

In this paper we present and discuss the procedures adopted to calibrate the detector and reconstruct the shower direction. Results concerning many shower features as the angular distribution, the density spectrum, the time profile of the shower front, are found well consistent with the expectation. © 2002 Elsevier Science B.V. All rights reserved.

PACS: 95.85.Pw; 96.40.Pq; 95.55.Ka; 95.55.Vj

Keywords: Gamma-ray astronomy; Cosmic rays; Ground-based astronomy; Extensive air shower; ARGO-YBJ

1. Introduction

The ARGO-YBJ¹ experiment is under way over the next few years at the Yangbajing High Altitude Cosmic Ray Laboratory (4300 m a.s.l., 606 g/cm^2 , longitude $90^\circ 31' 50'' \text{ E}$, latitude $30^\circ 06' 38'' \text{ N}$), 90 km north to Lhasa (Tibet, P.R. China). The aim of the experiment is the study of cosmic rays, mainly cosmic γ -radiation, at an energy threshold of $\sim 100 \text{ GeV}$ with a detector sampling the charged particles of atmospheric showers. Such a detector is capable of performing a continuous high sensitivity all-sky survey in the declination band $-10^\circ < \delta < 70^\circ$, thus complementing the narrow field of view air Cerenkov telescopes.

This goal can be achieved

- by operating the detector at very high altitude ($>4000 \text{ m a.s.l.}$) to increase the size of low energy showers;
- by using a full coverage layer of counters able to provide a high granularity sampling of shower particles.

The idea of detecting small size air showers forms the basis of the ARGO-YBJ experiment. The final apparatus will consist of a full coverage array of dimension $\sim 74 \times 78 \text{ m}^2$ realized with a single layer of resistive plate counters (RPCs), $280 \times$

125 cm^2 each. The area surrounding the central detector core, up to $\sim 100 \times 100 \text{ m}^2$, is partially ($\sim 50\%$) instrumented with RPCs. This outer ring improves the apparatus performance, enlarging the fiducial area for the detection of showers with the core outside the full coverage carpet. A lead converter 0.5 cm thick will cover uniformly the RPCs plane. In this way the number of charged particles is increased by conversion of shower photons, thus lowering the energy threshold and reducing the particle time fluctuations on the shower front. The RPC signals are picked up by means of strips 6 cm wide and 62 cm long. The strips ($124\,800$ in total in the carpet) are the basic element which defines the space pattern of the shower. The fast-OR signals of 8 strips are used for time measurements and trigger purposes. These OR-ed strips define a logic PAD of $56 \times 62 \text{ cm}^2$ ($17\,400$ in total), which is the basic element providing the time pattern of the shower. The basic detection unit will be the cluster, a set of 12

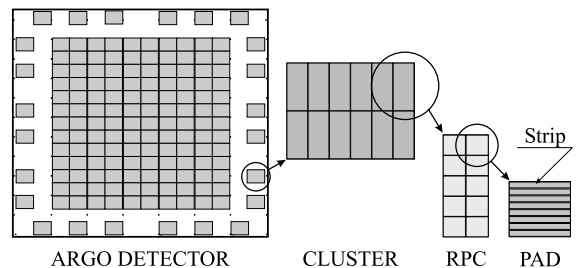


Fig. 1. Layout of the ARGO-YBJ array showing the definition of CLUSTER, RPC, PAD, Strip. The dimensions of these components are given in the text.

¹ Astrophysical Radiation with Ground-based Observatory at Yangbajing. ARGO is the name of a mythological monster, with several eyes, never sleeping.

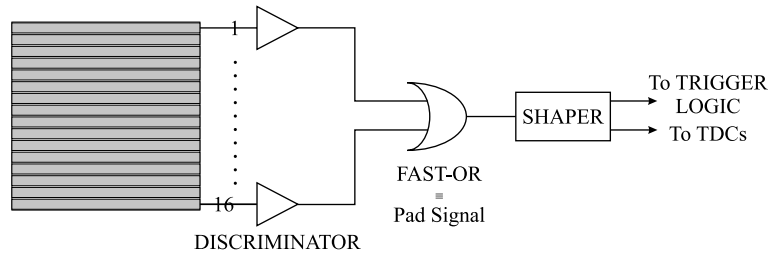


Fig. 2. The electronic block diagram of the strip signal processing.

contiguous RPCs (see Fig. 1). ARGO-YBJ will be housed in a building capable of keeping the temperature in the RPCs operating range ($\sim 5\text{--}25^\circ\text{C}$). Data taking with the first $\sim 750\text{ m}^2$ of RPCs will start in 2001.

This experiment will image with high efficiency and sensitivity atmospheric showers initiated by primaries of energies $\geq 100\text{ GeV}$, allowing to bridge the GeV and TeV energy regions and to produce data on a wide range of fundamental issues in cosmic ray physics and γ -ray astronomy [1,2].

In order to investigate both the RPCs performance at 4300 m a.s.l. and the capability of the detector of sampling the shower front of atmospheric cascades, during 1998 a cluster prototype of $\sim 50\text{ m}^2$ has been put in operation in the Yangbajing Laboratory. The results concerning the RPCs performance are given in paper [3]. In the following we describe the experimental set-up of this test experiment and discuss the results obtained from the analysis of data collected by means of a shower trigger. They concern primarily the angular distribution, the density spectrum, and the time profile of EAS in the energy range $10^{12}\text{--}10^{14}\text{ eV}$.

2. The test experiment at Yangbajing

The detector, consisting of a single gap RPC layer, is installed inside a dedicated building at the Yangbajing Laboratory. The set-up is an array of 3×5 chambers of area $280 \times 112\text{ cm}^2$ each, lying on the building floor and covering a total area of $8.6 \times 6.0\text{ m}^2$. The active area of 46.2 m^2 , accounting for a dead area due to a 7 mm frame closing the chamber edge, corresponds to a 90.6% coverage. The RPCs, with a 2 mm gas gap, are

built with bakelite electrode plates of volume resistivity in the range $(0.5\text{--}1) \cdot 10^{12}\ \Omega\text{cm}$, according to the standard scheme reported in Ref. [4].

In this test the RPCs signals have been picked up by means of 160 aluminium strips 3.3 cm wide and 56 cm long. At the edge of the detector the strips are connected to the front end electronics and terminated with $50\ \Omega$ resistors. The front end circuit contains 16 discriminators, with about 50 mV voltage threshold, and provides a FAST-OR signal (PAD signal) with the same input-to-output delay (10 ns) for all the channels. This signal is used for time measurements and trigger purposes in the present test. Each RPC is therefore subdivided in 10 pads (of $56 \times 56\text{ cm}^2$ area) which work like independent functional units (see Fig. 2).

In this test experiment the strip read-out has not been implemented. Therefore the pads are the basic elements which define the space-time pattern of the shower; they give indeed the position and the time of each detected hit.

The FAST-OR signals of all 150 pads are sent through coaxial cables of the same length to the carpet central trigger and read out electronics. The trigger logic allows events to be selected with a pad multiplicity in excess of a given threshold. At any trigger occurrence the times of all the pads are read out by means of multihit TDCs of 1 ns time bin, operated in COMMON STOP mode. Since the PAD signal is shaped to $1.5\ \mu\text{s}$ only the time profile of the earliest particles hitting each pad is imaged. The RPCs have been operated in streamer mode with gas mixtures of argon (15%), isobutane (10%) and tetrafluoroethane $\text{C}_2\text{H}_2\text{F}_4$ (75%), at a voltage of 7400 V, about 500 V above the plateau knee. The efficiency of the detector, as measured by a small telescope selecting a cosmic ray

beam, is $>95\%$, and the intrinsic time resolution $\sigma_t \sim 1$ ns.

A detailed description of many technical aspects concerning the detector assembly, the results of the measurements made on different gas mixtures and those concerning the RPCs performance at Yangbajing are given in Ref. [3].

3. Event reconstruction procedure

3.1. Trigger rate and shower density

Data was taken either with or without a 0.5 cm layer of lead on the whole carpet in order to investigate the converter effect on multiplicity and angular resolution. An inclusive trigger requiring at least 10 pads fired within 100 ns has been used to collect $\sim 10^6$ shower events in April–May 1998.

The integral trigger rate as a function of the number of hit pads per shower (pad multiplicity m) is shown in Fig. 3 or showers before and after the lead was installed. A comparison at fixed rate indicates an increase $\sim 15\text{--}20\%$ of the pad multiplicity due to the effect of the lead conversion.

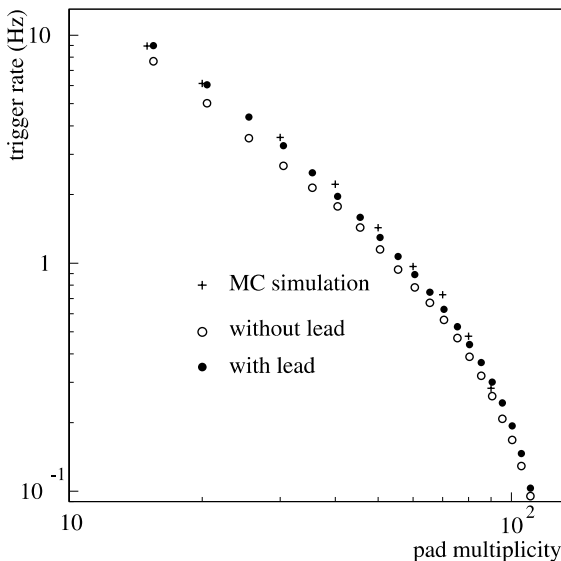


Fig. 3. The integral trigger rate as a function of the pad multiplicity compared to results of a Monte Carlo simulation taking into account the effect of the lead converter.

In Fig. 3 the experimental data is compared to the results of a simulation carried out by means of the CORSIKA code (version 5.624) [5]. CORSIKA uses EGS4 [6] for electromagnetic interactions, while different options are available for the hadronic ones. The GHEISHA [7] code is used for low-energy hadronic interaction ($E \leq 80$ GeV) and the HDPM interaction model for higher energies. The detector response has been simulated with the GEANT package (version 3.21) [8]. The energy of primary particles has been sampled from 500 GeV to 500 TeV for protons and between 1 and 500 TeV for helium nuclei. The absolute flux has been taken from Honda et al. [9]. The contribution of nuclei heavier than helium has been neglected.

The simulated showers are thrown with cores randomly distributed over an area 300×300 m². The zenith angle at the top of the atmosphere is uniformly sampled between 0° and 60° . Fig. 4 shows the contribution of protons and helium nuclei to the integral trigger rate at a pad multiplicity $m = 15$, as a function of the primary energy. The total rate predicted by the simulation is in fair agreement with the measured rate. The contribution

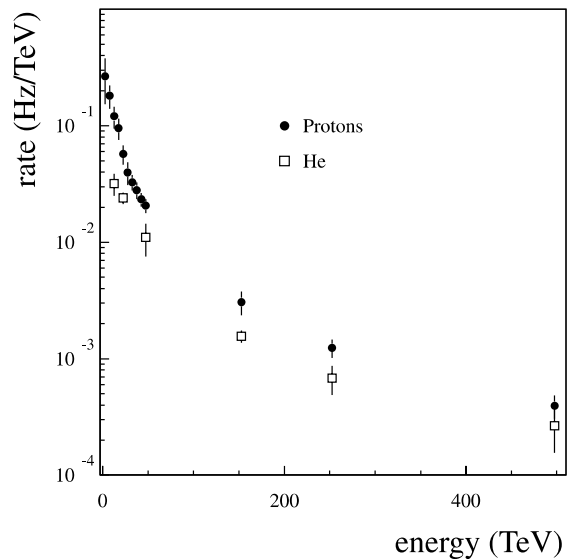


Fig. 4. The calculated contribution of protons and helium nuclei to the integral trigger rate at a pad multiplicity $m = 15$. Each point represents the average of many events generated over different energy ranges according to the spectra given in Ref. [9].

of the helium nuclei to the total trigger rate is found to be $\sim 29\%$. According to some limited-statistics simulations, the contribution from heavier nuclei is expected to be not greater than a few percent.

Since in this test the strip read-out is not performed, the actual multiplicity is underestimated for particle densities higher than $\sim 1 \text{ m}^{-2}$. The average particle density as a function of the recorded multiplicity has been obtained by the previous Monte Carlo simulation.

The average density ρ of charged particles of quasi-vertical ($\theta = 0\text{--}20^\circ$) showers hitting the lead-covered RPCs is shown in Fig. 5 as a function of pad multiplicity. Here ρ is the particle density averaged over the detector area, irrespective of the sizes and locations of the shower axes. A simulation of the detector response without lead plates shows a decreasing pad multiplicity at fixed particle density well consistent with data of Fig. 3.

Showers incident at zenith angle θ see pads of reduced size so that a dependence $\rho(\theta, m) = \sec \theta \rho(0, m)$ is expected. The validity of this relation is confirmed only approximately by the Monte Carlo simulation. A deviation is observed since the actual thickness of the lead converter increases with zenith angle. The particle density versus pad multiplicity for showers incident at zenith angle $\theta = 43\text{--}47^\circ$ is also reported in Fig. 5. These results have been used to convert the measured pad multiplicity to the average particle density.

Since in this experiment the shower size is not measured, events have been classified and analyzed with respect to pad multiplicity or average density. The analysis has been restricted to events with $m \geq 20$ and $\rho \leq 10 \text{ particles/m}^2$ in order to avoid either threshold or saturation effects.

3.2. Detector calibration

The accuracy in the reconstruction of the shower arrival direction mainly depends on the capability of measuring the relative arrival times of the shower particles. This direction is obtained after reconstructing the time profile of the shower front by using the information from each timing pixel (pad) of the detector. The time resolution of each pad ($\sim 1.3 \text{ ns}$) is determined by the RPC intrinsic time resolution, the propagation time of the signal

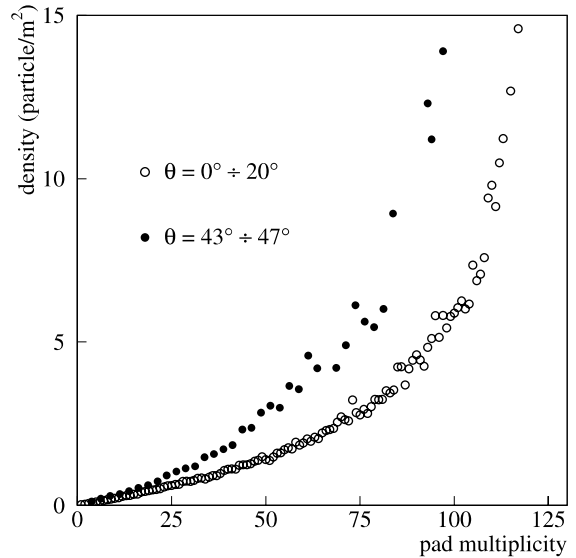


Fig. 5. Average particle density as a function of the measured multiplicity for showers incident at different intervals of zenith angle. Each point represents the average of many showers contributing to a given pad multiplicity.

traveling along a strip of 56 cm and the electronic time resolution. Data concerning the performance of the pad read-out is presented in Ref. [3].

An additional factor derives from the timing offset between different channels due to differences in the time discharge of the RPCs, different cable delays and other instrumental effects. Differences in propagation delay in the signal cables and in the printed circuits have been properly accounted for. A sample of time distributions is shown in Fig. 6. The relative timing offset among different pads has been determined as follows:

- (1) The time distribution of each TDC channel is built-up by adding all the delays recorded.
- (2) The timing offset for each TDC channel is obtained by comparing the peak of the TDC spectrum to a reference channel one. These timing offset are used to correct time data.
- (3) Events are reconstructed following the procedure of Section 3.3. Well reconstructed, quasi-vertical events are selected by requiring reduced $\chi^2 < 10$, zenith angle $\theta < 15^\circ$.

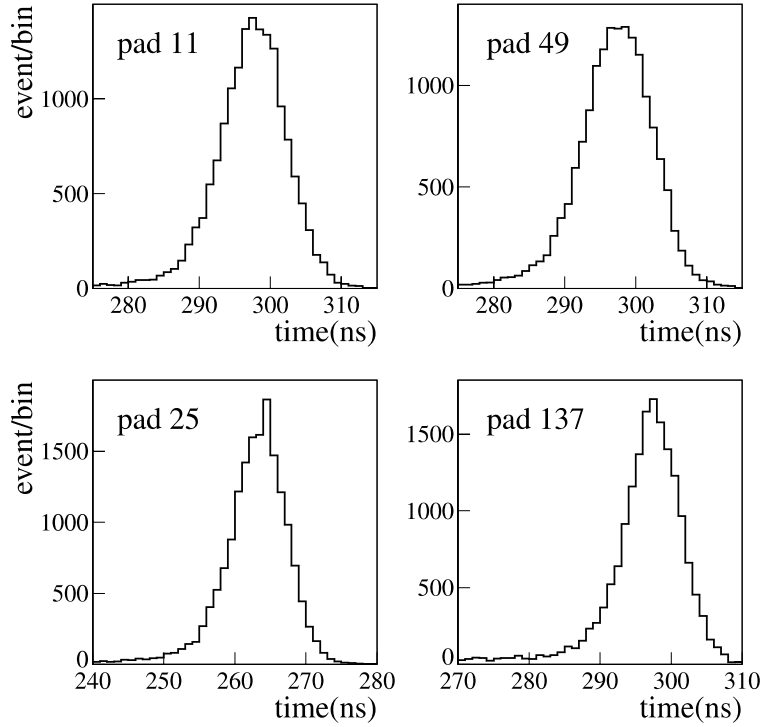


Fig. 6. Typical time distributions for 4 TDC channels (i.e. pads).

(4) The procedure of steps (1) and (2) is repeated on data of this subset to obtain the final set of timing offsets.

To check the consistency of the procedure, the corrected times in events belonging to the selected sample have been fitted to a plane and the distribution of time residuals $\delta t_i = t_{\text{plane}} - t_i$ has been obtained for each TDC channel. The time corresponding to the peaks of these distributions are spread with a width of ~ 0.6 ns.

3.3. Event reconstruction

Shower particles are concentrated in a front of parabolic shape. A good approximation for particles not far from the shower core is represented by a cone-like shape with an average cone slope of about 0.10–0.15 ns/m [10,11]. Since in this test the signals sent to TDCs are shaped to 1.5 μs only the time of the first particle hitting each pad is recorded. According to the results of simulations

tuned to the Yangbajing depth [10,11] the foremost particles are expected to be concentrated in a shower front of conical shape, within 40 m from the core, with a slope of about 0.013 ns/m.

However, due to the reduced size of the detector, the time profile of the shower front sampled by the carpet is expected to exhibit a planar shape. In this approximation the expected particle arrival time is a linear function of the position. The time profile observed in a typical event is shown in Fig. 7. Here x and y are orthogonal coordinates which identify the pad position. Straight lines are one-dimensional fits to experimental hits along two different x values. The algorithm that reconstructs the arrival direction of the shower fits the times and locations of each hit to a plane by χ^2 minimization. The distribution of the arrival times shows non-Gaussian tails at later times, mainly due to multiple scattering of low energy electrons but also to incorrect counters calibrations and to random coincidences. These non-Gaussian tails are expected typically to be $\sim 20\%$ of all measured

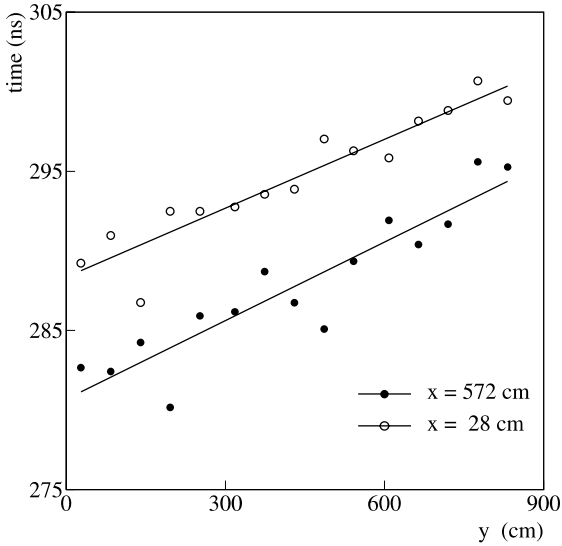


Fig. 7. Time profile observed in a typical event. Straight lines are fit to experimental hits. x and y are orthogonal coordinates which identify the center of each pad.

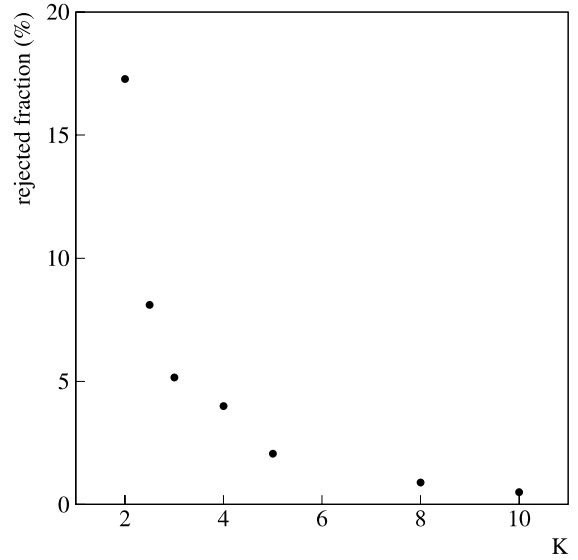


Fig. 8. The percentage of discarded hits as a function of the cutting value K .

time values. It is important to take properly into account these extreme time fluctuations in order to not worsen the reconstruction of the direction. The following procedure has been adopted [12,13]:

- Unweighted plane fit to hits for each event by minimization of the function

$$\Psi^2(ns^2) = \frac{1}{c^2} \sum_i \{lx_i + my_i + nz_i + c(t_i - t_0)\}^2 \quad (1)$$

The sum includes all pads with a time signal t_i , c is the light velocity, (x_i, y_i, z_i) are the central position of the i th pad. The parameters of the fit are the time offset t_0 and the l, m direction cosines.

- Rejection of outlying times by means of a $K \cdot \sigma$ cut and iteration of the fit until all times verify this condition or the remaining hits number is ≤ 5 (in this case the event is discarded). Here σ is the standard deviation of the time distribution around the fitted plane.

This procedure is rather fast because it makes use only of analytic formulae. No a priori information about shower features is required. The actual value of K could depend on the features of

the reconstructed showers as well as on the experimental condition (pad dimension, shaping of the signals, multihit capability, etc.). By choosing $K = 2.5$ about 8% of the hits are rejected (Fig. 8). Decreasing K should increase the number of discarded hits without a significant improvement of the χ^2 . The normalized χ^2 distribution ($\chi^2 = \Psi^2/\text{d.o.f.}$) for two multiplicity range is presented in Fig. 9. The dashed histograms refer to the χ^2 distribution after the first step of the fitting procedure. Rejecting the most deviating hits tightens the distributions as shown by the continuous lines. In these curves the quantity $(\chi^2)^{1/2}$ represents (approximately) the average time spread. Thus the peak of the distributions corresponds to events where hits are about 2 ns scattered around the fitted plane. These distributions exhibit a long tail more pronounced for low multiplicity events and not completely cut out by the optimized fitting procedure. In these events the time hits are considerably spread, by far more than expected from the detector time resolution. They can be attributed to the sampling of a portion of the shower affected by large time fluctuations.

The average χ^2 are plotted in Fig. 10, for events with and without the 0.5 cm lead plane on the

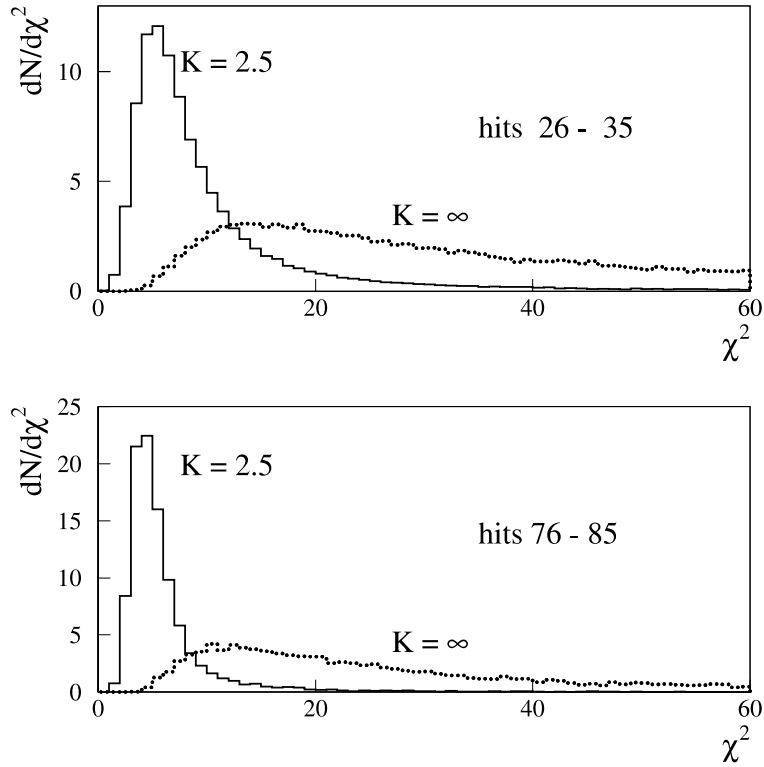


Fig. 9. The χ^2 distribution without (dashed line) and with (continuous line) cutting for two multiplicity range.

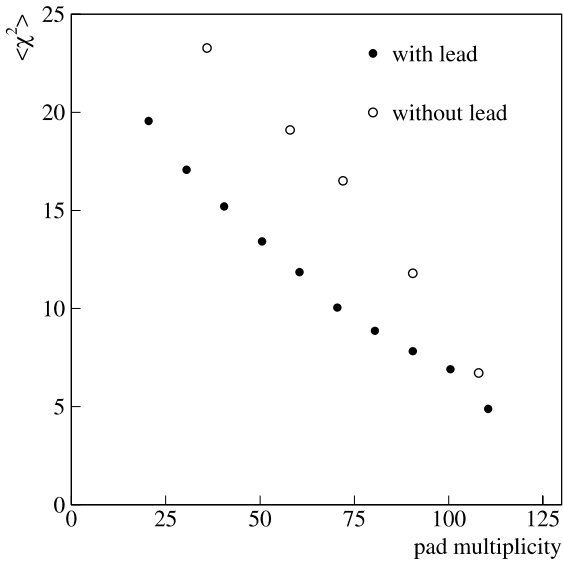


Fig. 10. The average χ^2 vs. pad multiplicity.

carpet (filled circles and crosses, respectively). The effect of the converter is well evident, consisting in a shrinking of the shower time thickness. This is expected since the lead absorbs low energy electrons, that mostly cause the non-Gaussian tails of the time distribution, and converts the shower photons. The improvement decreases with increasing multiplicity.

Events with $\chi^2 > 30$ (about 10% of the total) have been discarded and not used in the following analysis.

4. Results

4.1. Angular distribution of shower events

The accurate determination of the atmospheric shower event rate as a function of the local coordinates (θ – zenith angle, ϕ – azimuthal angle) is of

great importance in many respects. For instance, in ground based gamma ray astronomy air showers from cosmic rays form the main source of background. When searching for weak signals from point astrophysical sources it is important to estimate the size of this background in an unbiased manner.

The event rate as a function of the zenith angle scales as $dN/d(\cos \theta) \propto \exp[-\alpha \sec \theta]$, due to atmospheric absorption, with the coefficient α related to the attenuation length of EAS. On the contrary, the azimuthal angle distribution is expected to be uniform within statistical fluctuations, $dN/d\phi = \text{const}$. In fact, since at the energies involved in this experiment cosmic rays are highly isotropic, no preferred directions are expected in local coordinates. An uniform, horizontal detector as ARGO-YBJ should have the average shower direction straight up. However, systematic time shifts could produce an apparent tilt of the horizontal plane and, consequently, a quasi-sinusoidal modulation of the azimuthal angle distribution [14]. Moreover, also trigger biases due to specific experimental conditions may cause the detection efficiency to be non-uniform in local coordinates. Deviation from the expected distribution can be considered as signs of some fault in the experimental setup. Thus, studying the EAS angular distribution provides information on the longitudinal shower development and allows an overall check of the detector performance and of the efficiency of the reconstruction algorithms.

4.1.1. The zenith angle distribution

The zenith angle distribution of events in various intervals of shower size has been extensively used to study the absorption in atmosphere of EAS generated by primaries with different energies. In the present experiment, where the measured particle density is due to the contribution of showers within a very broad range of sizes, the study of the angular distribution of events with particle density exceeding a given value, appears more appropriate. The angular distribution is expected to follow an exponential behaviour

$$I(\geq \rho, \theta) = I(\geq \rho, 0) \exp\left(-\frac{x_0}{A_{\text{att}}}(\sec \theta - 1)\right) \quad (2)$$

where x_0 is the vertical depth and A_{att} is the attenuation length of showers with particle density exceeding ρ .

According to numerous measurements from sea level to an altitude of about 4 km, A_{att} lies between 120 g/cm² and 150 g/cm² for showers with moderate size [15,19]. Thus the exponent of the angular distribution measured at Yangbajing is expected in the range 4–5.

The validity of this expression extends over an angular range where the atmospheric overburden increases as $1/\cos \theta$ and the decay path of mesons is larger than the interaction path so that absorption in atmosphere dominates the shower development. Data recorded in various experiments at different altitude is consistent with Eq. (2) for $\theta_{\text{max}} \leq 60^\circ$ [16–18].

The angular distribution of events with density greater than 3 particles/m² is shown in Fig. 11. The data can be fit out to $\sim 55^\circ$ with an $\exp[-\alpha \cdot (\sec \theta - 1)]$ law. The parameter α is found to be 4.88 ± 0.45 , so that $A_{\text{att}} = (124 \pm 11)$ g/cm², in excellent agreement with previous results. For comparison, the value provided by Monte Carlo simulations is 4.11 ± 0.37 . For angles greater than

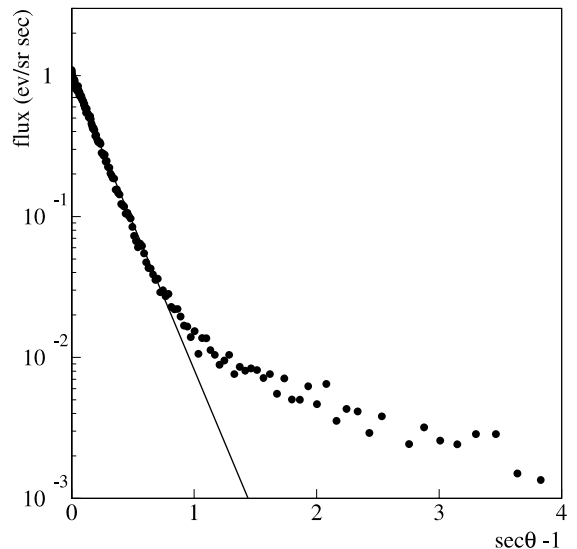


Fig. 11. Zenith angle distribution of showers with $\rho \geq 3$ particle/m². The solid line shows the exponential behaviour of the angular distribution of primary cosmic rays.

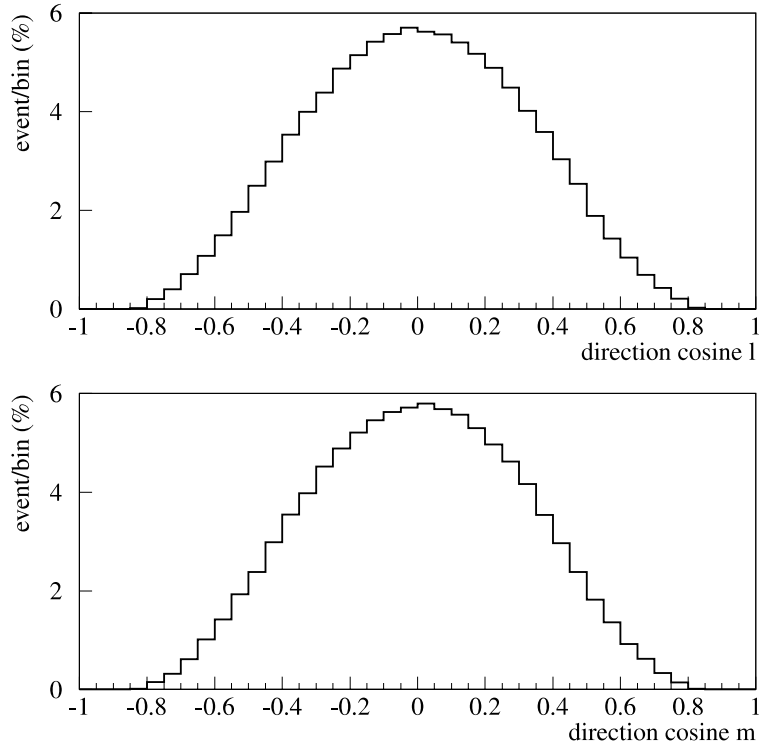


Fig. 12. Distribution of the direction cosines.

55° a deviation from this law is observed. Misreconstructed events, showers locally produced in the walls of the surrounding buildings and horizontal air showers could contribute to these large angle events. This data confirms that the shape of the zenith angle distribution is dominated by the physical effect of atmospheric absorption.

4.1.2. The azimuthal angle distribution

The presence of systematic timing inaccuracies or trigger biases artificially producing asymmetries in the air shower arrival direction can be inferred by checking the uniformity of the azimuthal distribution.

However, since in the ARGO-YBJ test experiment the detectors (pads) are placed on a rectangular grid with sides running along the x and y coordinates, it results more convenient to determine the distribution of the shower events as a

function of the direction cosines $l = \sin \theta \cos \phi$ and $m = \sin \theta \sin \phi$. These distributions are expected to be symmetric around $\langle l \rangle = \langle m \rangle = 0$.

This is verified for the data subset of quasi-vertical events used to determine the relative timing delay of each TDC channel ($\chi^2 < 10, 0^\circ \leq \theta \leq 15^\circ$). The distribution of all selected events ($\chi^2 \leq 30, 0^\circ \leq \theta \leq 55^\circ$) is shown in Fig. 12.

The average values of direction cosines l and m are found to be -0.0003 ± 0.0005 and -0.0005 ± 0.0005 , respectively. These distributions both exhibit a symmetric shape suggesting that residual systematic timing shifts are negligible.

However, the distributions look slightly different at very large zenith angles. This is a mere geometrical effect due to the rectangular shape of the detector. In fact, while the sampling area seen by a shower incoming from a direction (θ, ϕ) depends only on the zenith angle θ , its shape is a function also of the azimuthal angle ϕ . Due to the density gradient

of the shower lateral distribution, different shapes may produce different trigger efficiencies. The effect becomes detectable at very large zenith angle.

4.2. The density spectrum

In the past several experiments were done on the density spectrum of EAS in order to gather information on the size spectrum. In fact, although the relation between the particle density spectrum and the shower size spectrum is quite complicated due to the large range of sizes contributing to events with a given particle density, in first approximation both spectra follow a power law with the same spectral index.²

According to the data of the Greisen review [19] the exponent β_i of the integral density spectrum changes very little with altitude and particle density. At mountain elevations (>3000 m a.s.l.) a dependence $\beta_i = 1.25 + 0.065 \log \rho(\text{m}^{-2})$ represents quite well the experimental data in the density range $\rho = 1 - 10^4 \text{ m}^{-2}$.

The differential density spectrum in the range 1–10 particles/m² has been measured at Yangbajing in different intervals of zenith angle. Data has been subdivided in 12 angular bins of with $\Delta \sec \theta = 0.05$ up to $\sec \theta = 1.5$ and $\Delta \sec \theta = 0.10$ in the $\sec \theta$ range 1.5–1.7. With this choice the atmospheric thickness increases by a constant amount, about 30 and 61 g/cm² respectively. The density spectrum for some intervals of zenith angle is shown in Fig. 13. The spectra refer to the depth corresponding to the mean zenith angle of the shower events recorded inside each interval. The shapes of the spectra are very similar in the density range 2–10 particles/m² not affected by threshold or saturation effects. The differential spectral index β is shown in Fig. 14 as a function of the zenith angle. A weighted mean up to $\theta < 45^\circ$ gives $\langle \beta \rangle = 2.26 \pm 0.07$, a value fairly consistent with the expectation. Events recorded at larger zenith angles ($>45^\circ$) are due to showers developed through at-

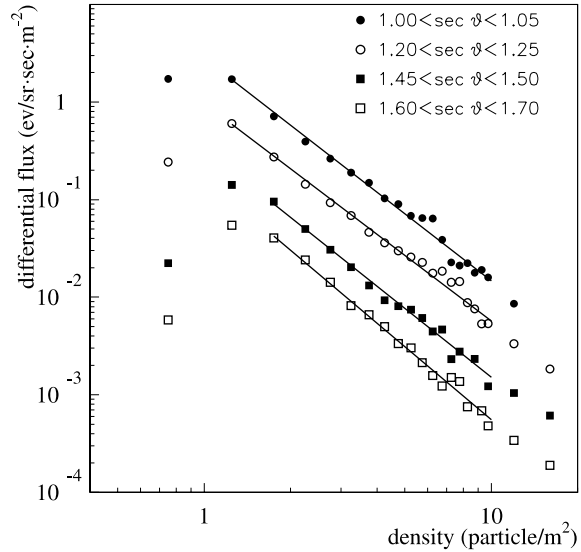


Fig. 13. Differential density spectrum measured at different intervals of zenith angle. The lines show the results of the fitting procedure.

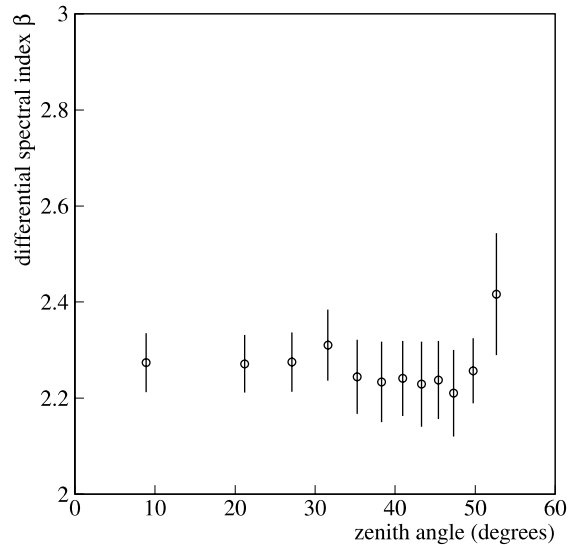


Fig. 14. The spectral index β of the differential density spectrum as a function of the zenith angle.

mospheric depths greater than 860 g/cm². Since for these events an increasing contribution is expected from showers originated by primaries of energies beyond the knee of cosmic ray spectrum, they have not been taken into account in this analysis.

² The exponent β of the density spectrum coincides with the exponent γ of the size spectrum if both the lateral distribution and the exponent of the size spectrum do not depend on the shower size N_e . As a matter of fact, $\beta < \gamma$ (see Ref. [19]).

Monte Carlo simulations show that present data concerns showers from primaries with energies ranging from 1–10 TeV (quasi-vertical showers) to a few hundred TeV (large zenith angles). Accordingly, the spectral index β can be considered a reasonable estimate of the average slope of the density spectrum measured at great altitude, for showers initiated by primaries (mainly protons) of energies $\sim 10^{12} - 10^{14}$ eV. A lower limit to the absorption length of EAS particles is found, $A_e > \beta_i A_{att} = 156 \pm 19$ g/cm² consistent with results concerning showers of small size [15].

4.3. Shower front thickness

The distribution of the times with respect to the fitted plane is shown in Fig. 15 for two different multiplicity ranges. Quasi-vertical showers ($\theta < 15^\circ$) have been selected. In order to make easier the comparison between these distributions, the one concerning events at lower multiplicity has been shifted of 0.4 ns. In such a way the peaks of the two distributions coincide. However, the time residual corresponding to the peak is not zero since the event reconstruction procedure of Section 3.3 does not symmetrize completely the experi-

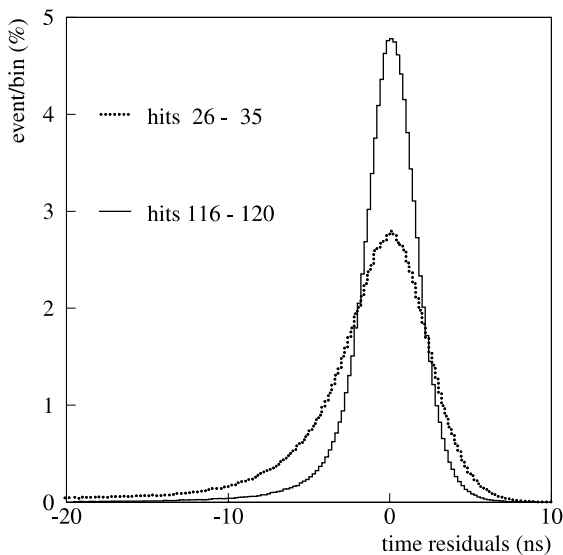


Fig. 15. Distribution of time residuals for events with different pad multiplicity (all channel added).

mental time distribution. The distribution of time residuals exhibits a long tail, more pronounced for low multiplicity events, due to time fluctuations and to the curved profile of the shower front. The width of these distributions is related to the time thickness of the shower front. Since the position of the shower core is not reconstructed, the experimental result concerns a time thickness averaged on different radial distances. Increasing pad multiplicity selects showers with the core near the detector.

In Fig. 16 the full width half maximum (FWHM) of the time residual distribution as a function of the pad multiplicity is shown. For low multiplicity events, with a mean number of particles per pad < 1 ($m \leq 80$), the FWHM represents a reasonable measurement of the shower thickness. For high multiplicity events ($m > 100$), where the mean number of particles hitting one pad is > 1 , the spread is not related to the thickness of the shower disc without any bias. In this case the time residual distribution is related to the fluctuations of the foremost particle hitting each pad. Taking into account the total detector resolution of 1.3 ns (RPC intrinsic jitter, strip length, electronics time resolution) the time jitter of the earliest particles in

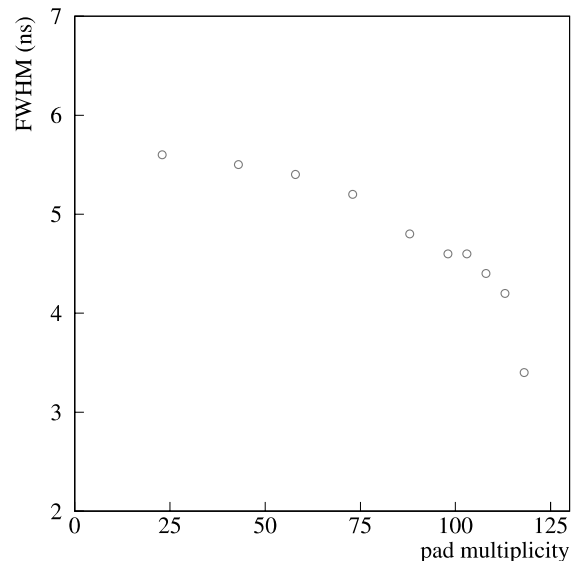


Fig. 16. The FWHM of the time residual distribution vs. the pad multiplicity.

high multiplicity events (>100 hits) is estimated ~ 1 ns. This value is in good agreement with the results of Monte Carlo calculations given in Ref. [10,11] for photon-initiated showers simulated at the Yangbajing atmospheric depth.

4.4. Angular resolution

The angular resolution of the carpet has been estimated by dividing the detector into two independent sub-arrays (“odd pads” and “even pads”) and comparing the two reconstructed shower directions. These two sub-arrays overlap spatially so that they sample the same portion of the shower. Events with m total pads have been selected according to the constraint $m_{\text{odd}} \simeq m_{\text{even}} \simeq m/2$. The distribution of the even–odd angle difference $\Delta\theta$ is shown in Fig. 17 for events in two multiplicity ranges and $\theta < 55^\circ$, $\chi^2 < 30$. These distributions follow fairly well, apart from a long tail, a Gaussian shape. They narrow, as expected, with increasing shower size. Assuming that the angular resolution function for the entire array is Gaussian, its standard deviation is given by $\sigma_\theta = M_{\Delta\theta}/2.354$, being $M_{\Delta\theta}$ the median of the distribution of the even–odd angle difference $\Delta\theta$ [20]. The

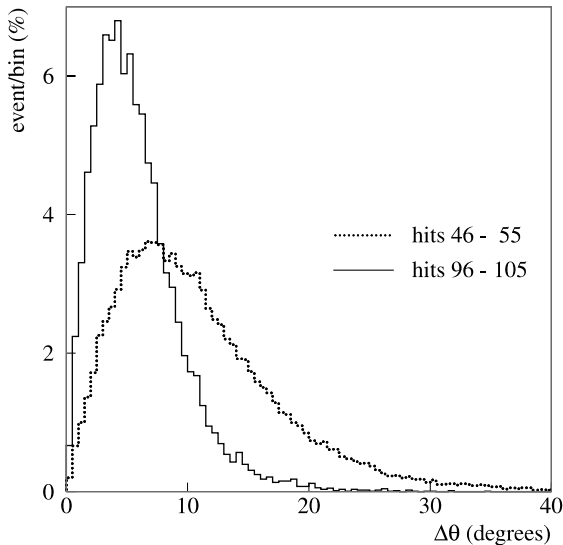


Fig. 17. Distribution of the even–odd angle difference $\Delta\theta$ for events with different pad multiplicity, in the case of lead-covered RPCs ($\theta < 55^\circ$, $\chi^2 < 30$).

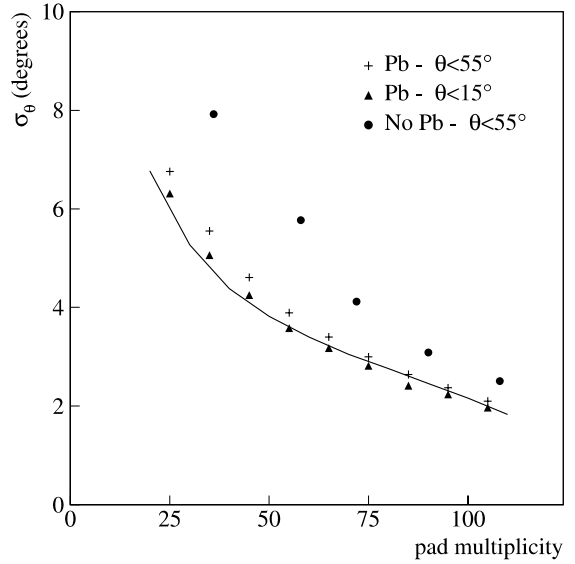


Fig. 18. The standard deviation σ_θ of the distribution of $\Delta\theta$ as a function of pad multiplicity. The curve represents a fit of Eq. (3) to data, for quasi vertical events.

angular resolution σ_θ is shown in Fig. 18 as a function of pad multiplicity, for showers reconstructed before and after the lead was added. The effect of the lead sheet can be appreciated.

Following the same arguments as given in Ref. [21], the angular resolution σ_θ , averaged on the azimuthal angle ϕ , is found to depend on pad multiplicity m and zenith angle θ as

$$\sigma_\theta(m, \theta) \propto \frac{\sigma_t(m)}{\sqrt{m}} \sqrt{\sec \theta} \quad (3)$$

where $\sigma_t(m)$ is the average time fluctuation for events with m hits. The factor $(\sec \theta)^{1/2}$ accounts for the geometrical effect related to the reduction with increasing θ of the effective distance between pads. The time spread $\sigma_t(m)$ can be inferred from the FWHM curves given in Fig. 16 as a function of m , for quasi-vertical events. As shown in Fig. 18, the angular resolution σ_θ for this sample of events is in satisfactory agreement with the Eq. (3). Thus, the dependence of σ_θ upon m is well explained in terms of the combined effect of the time thickness of the EAS disk, as imaged by the detector, and the density of shower particles.

The angular resolution σ_θ expected from the Monte Carlo simulations is found to be about 20% better than the one shown in Fig. 18. The origin of this discrepancy is due to the fact that simulated data does not correctly account for the events with a large time spread. These events are responsible for the tails of the distributions shown in Fig. 17. A straightforward interpretation is that simulated air showers fail to fully reproduce the time fluctuations of particles at large distances from the core. However, since in the experiment the shower core position is not reconstructed this explanation cannot be proved. The agreement is restored once the comparison is carried out for events with $\chi^2 < 10$.

5. Conclusions

In view of an extensive use in the ARGO-YBJ experiment, a 50 m² RPCs carpet has been operated in the Yangbajing laboratory with the aim of checking the detector capability of imaging the front of atmospheric showers. In this test the logic element (“pixel”) for both space and time sampling has been a PAD of 56 × 56 cm² area. Data collected with a shower trigger at zenith angles $\theta < 45^\circ$ is mainly originated by primaries in the energy range 10¹²–10¹⁴ eV. A general procedure for detector calibration and event reconstruction has been implemented. Shower events with particle density in the range 1–10 particles/m² have been analyzed to determine the angular distribution, the density spectrum and the time profile of the shower front. Though the dimension of the test carpet is somewhat too small for EAS observation, many relevant features of atmospheric showers have been measured, as the absorption length of EAS particles, the average shower thickness and the time fluctuation of the foremost particle hitting each pad. The angular resolution has been inferred by dividing the carpet into two independent, interlocking PAD subsets. The effect of adding 0.5 cm of lead has been investigated.

The results of this test show that (i) RPCs can be operated efficiently ($\geq 95\%$) to sample air showers at high altitude with excellent time resolution (~ 1.3 ns including electronics); (ii) an appropriate

calibration procedure may reduce systematics below the intrinsic time resolution of the detector; (iii) the RPCs carpet and the signal read-out by means of pick-up strips envisaged for this experiment may provide a highly detailed picture of the space-time pattern of the shower front; (iv) the effect of the lead sheet of reducing time fluctuations is confirmed.

The accuracy of shower parameter reconstruction turns out to be as good as one may expect from the high density sampling and from the performance of the detector. Thus the overall results of the test look well promising for future operation of the full ARGO-YBJ detector.

Acknowledgements

The authors wish to thank P. Parascandolo, G. Pellizzoni, C. Pinto, E. Reali, and S. Stalio for their continuous technical assistance. This work is supported partly by the Chinese Academy of Sciences, the Ministry of Science and Technology and the National Science Foundation of China.

References

- [1] M. Abbrescia et al., *Astroparticle Physics with ARGO Proposal*, 1996.
- [2] C. Bacci et al., *The ARGO-YBJ Project, Addendum to the Proposal*, 1998. These unpublished documents can be downloaded at the URL: <http://www1.na.infn.it/wsubnucl/cosm/argo/argo.html>.
- [3] C. Bacci et al., *Nucl. Instr. Meth. A* 443 (2000) 342.
- [4] *ATLAS Muon Spectrometer Technical Design Report*, CERN/LHCC/97-22 (Chapter 8).
- [5] D. Heck et al., *Report FZKA 6019*, Forschungszentrum Karlsruhe, 1998.
- [6] W.R. Nelson et al., *SLAC Report*, 1985, p. 265.
- [7] H. Fesefeldt, *Report PITHIA-85/02*, RWTH Aachen, 1985.
- [8] CERN Application Software Group, CERN W, 5013, version 3.21, 1994.
- [9] M. Honda et al., *Phys. Rev. D* 52 (1995) 4985.
- [10] B. D’Ettorre Piazzoli, G. Di Sciascio, *Astropart. Phys.* 2 (1994) 199.
- [11] G. Di Sciascio, B. D’Ettorre Piazzoli, M. Iacovacci, *Astropart. Phys.* 6 (1997) 313.
- [12] D. Campana, B. D’Ettorre Piazzoli, G. Di Sciascio, *Nucl. Instr. Meth. A* 344 (1994) 250.

- [13] H. Krawczynski et al., Nucl. Instr. Meth. A 383 (1996) 431.
- [14] A.M. Elo, H. Arvela, Proc. 26th ICRC, Salt Lake City, vol. 5, 1999, p. 328.
- [15] S. Bennet et al., J. Phys. Soc. Jpn. 17 (Suppl. A-III) (1961) 196.
- [16] D.E. Alexandreas et al., Nucl. Instr. Meth. A 328 (1992) 570.
- [17] M. Aglietta et al., Nucl. Phys. B (Proc. Suppl.) 70 (1999) 509.
- [18] D. Berley et al., Proc. 25th ICRC, vol. 5, Durban, 1997, p. 201.
- [19] K. Greisen, Ann. Rev. Nucl. Sci. 10 (1960) 63.
- [20] D.E. Alexandreas et al., Nucl. Instr. Meth. A 311 (1992) 350.
- [21] A. Karle et al., Astropart. Phys. 3 (1995) 321.